ISSN 2070-0482, Mathematical Models and Computer Simulations, 2012, Vol. 4, No. 2, pp. 229–235. © Pleiades Publishing, Ltd., 2012.
Original Russian Text © E.N. Bereslavskii, 2011, published in Matematicheskoe Modelirovanie, 2011, Vol. 23, No. 9, pp. 3–13.

A Way to Calculate the Seepage Attached to the Flow around the Zhukovskii Rabbet with More Than One-Sheeted Area of Complex Velocity

E. N. Bereslavskii

GOUVPO Saint-Petersburg State University of Civil Aviation, St. Petersburg, Russia
e-mail: eduber@mail.ru

Received April 19, 2011

Abstract—Under the definition of a hydrodynamic problem, a problem is solved on flat steady-state seepage under a Zhukovskii rabbet through irrigated soil bedded by a very permeable pressure horizon, whose left semi-infinite roof is simulated by an impenetrable inclusion. The movement in the case when the velocity of the flow at the rabbet's end is equal to infinity, which causes more than one sheeted area of complex velocity, is examined. The results are compared with the results obtained for the case when the velocity of the flow at the rabbet's end is a finite quantity.

Keywords: seepage, Zhukovskii rabbet, ground water, infiltration, Polubarinova-Kochina method, flow complex velocity, conformal mapping.

DOI: 10.1134/S2070048212020032

1. INTRODUCTION

The fluid flow under a Zhukovskii rabbet through irrigated soil bedded by very permeable pressure horizon, whose left semi-infinite roof is simulated by an impenetrable inclusion, is examined. To study the seepage process to a free surface, it is assumed that the velocity of the flow at the rabbet's end is a finite quantity and meets the following condition: $0 < |\overline{v}_G| < \varepsilon$, where ε $(0 < \varepsilon < 1)$ is the infiltration's uniform intensity related to soil seepage coefficient $\kappa = \text{const}$.

Below, we investigate the case when the velocity of the flow at the rabbet's end is accepted as infinite. In this case, the area of complex velocity is not one-sheeted in contrast to the case described in [1], where the area of the complex velocity is one-sheeted. The Polubarinova-Kochina method [2, 3] and also the procedures of conformal mapping [4–6] for special areas, which are typical for the problems of underground hydromechanics [7–9] are used to solve the mixed multi-parametric boundary problem. The exact analytical representations for characteristic sizes of flow motion are obtained. On the base of this model, an algorithm for calculating the ground water height behind the rabbet, coordinates of depression curve points, and other parameters of the flow is developed. The hydrodynamic analysis of the structure and typical peculiarities of the simulating process is performed with the help of numerical calculations. There are limit cases of flow motion since there is no impermeable inclusion or upthrust in the bottom very permeable aquifer. The results are compared with the results obtained for the case of a finite velocity of the flow at the end of the rabbet [1].

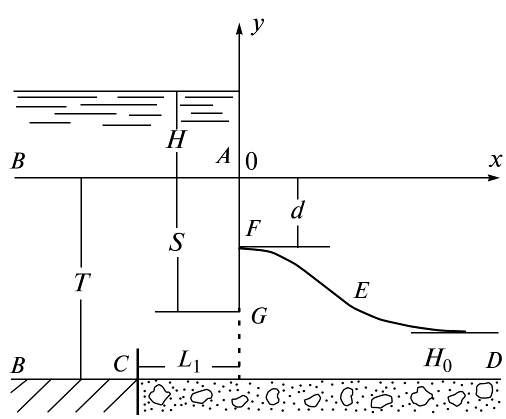

Fig. 1. Flow pattern for the flow around the Zhukovskii rabbet in the irrigated soil bedded by a very permeable pressure horizon.

2. PROBLEM DEFINITION

Figure 1 depicts schematically the flow pattern. As before [1], we examine a flat steady-state motion of incompressible fluid according to Darcy's law in uniform and isotropic soil through a soil layer of power T towards a very permeable aquifer with constant water head H_0 and for this case the left semi-

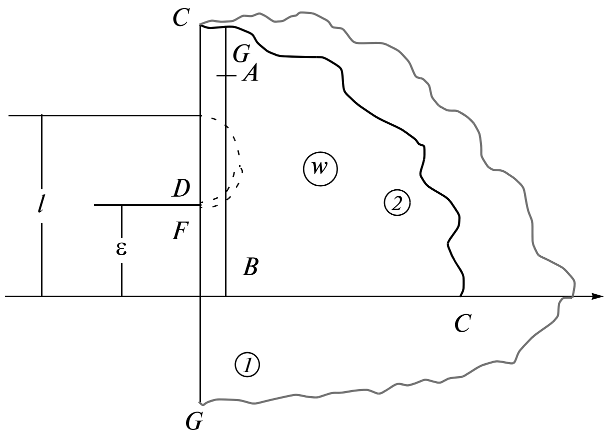

Fig. 2. Area of complex velocity *w*.

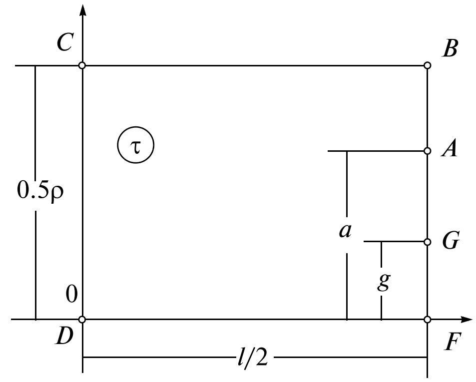

Fig. 3. Area of auxiliary parametrical variable τ.

infinite part of the roof *BC* is simulated by a water-proof inclusion. The moving water flowing around the rabbet rises at a certain height *GF* and forms a free surface *DF*, to which the infiltrated water flows with intensity ε. In the examined case, the velocity of the flow at the rabbet's end is infinite, in contrast to [1], where the peak of this velocity is limited by value ε.

Let us introduce the complex potential of motion $\omega = \varphi + i\psi$, where φ is a velocity potential, ψ is a flow function, and the complex coordinate $z = x + iy$ is related κH and H, respectively. Under such assumptions, traditional for the examined class of flows, the process of seepage simulation is reduced to the problem of how to find the complex potential $\omega(z)$ under the following boundary conditions:

$$\begin{aligned} &AB: y = 0,\ \varphi = -H;\ BC: y = -T,\ \psi = 0;\ CD: y = -T,\ \varphi = 0; \\ &DF: \varphi = -y + H_0 - T,\ \psi = \varepsilon x + Q;\ AF: x = 0,\ \psi = Q, \end{aligned} \tag{1}$$

where Q is the seepage flow rate. The procedure for determining the water height *GF* behind the rabbet, i.e., $S - d$, is of great interest.

3. SOLUTION

Despite the fact that the boundary conditions of the problem coincide with the boundary conditions for the case $|\overline{v}_G| < \varepsilon$; here, the structure and area of complex velocity presented in Fig. 2 are changed drastically. This area, belonging to the class of polygons in polar grids [8, 10], becomes two-sheeted (in contrast to the case examined in [1]), and if we travel along the boundary, at points *C* and *G*, we pass to the second Riemann sheet and back.

By considering specific properties of the areas in polar grids caused by right angles and cuts, it is convenient to accept the rectangle of plan τ as a canonical domain [11] (Fig. 3):

$$0 < \operatorname{Re}\tau < 0.5,\ 0 < \operatorname{Im}\tau < 0.5\rho,\ \rho(k) = K'/K,\ K' = K(k'),\ k' = \left(1 - k^2\right)^{1/2},$$

where $K(k)$ is a complete elliptical integral of the first kind for module k [12]. Using the procedure for generating the mapping functions for similar domains [4–6], let us determine the following expression for the function that performs the conformal mapping of the auxiliary rectangle of plane τ into an area of complex velocity:

$$w = \sqrt{\varepsilon}\, i \frac{\left(1 + \sqrt{\varepsilon}\right)\exp(\pi\tau i)\vartheta_1(\tau + i\gamma)\vartheta_2(\tau - i\alpha)\vartheta_2(\tau + i\beta) + \left(1 - \sqrt{\varepsilon}\right)\exp(-\pi\tau i)\vartheta_1(\tau - i\gamma)\vartheta_2(\tau + i\alpha)\vartheta_2(\tau - i\beta)}{\left(1 + \sqrt{\varepsilon}\right)\exp(\pi\tau i)\vartheta_1(\tau + i\gamma)\vartheta_2(\tau - i\alpha)\vartheta_2(\tau + i\beta) - \left(1 - \sqrt{\varepsilon}\right)\exp(-\pi\tau i)\vartheta_1(\tau - i\gamma)\vartheta_2(\tau + i\alpha)\vartheta_2(\tau - i\beta)}, \tag{2}$$

where ϑ_1 and ϑ_2 are the first and second theta-functions with parameter $q = \exp(-\pi\rho)$, which is connected unambiguously with module k [12]; α, β, and γ are the unknown constants of the conformal mapping that binds by the following relationship $\operatorname{th}\pi(0.5\rho + \alpha - \beta - \gamma) = \sqrt{\varepsilon}$. To solve boundary problem (1), let us use the Polubarinova-Kochina method [2, 13, 14], the main idea of which is to use the analytical theory of the Fuchs linear differential equations [15].

By using the procedure for determining the functions' characteristic measures $d\omega/d\tau$ and $dz/d\tau$ near nonsimple points [2, 3, 14, 15] and by considering Eq. (2) and $w = d\omega/dz$, we can write

$$\frac{d\omega}{d\tau} = -\sqrt{\varepsilon}M$$
$$\times \frac{\left(1+\sqrt{\varepsilon}\right)\exp(\pi\tau i)\vartheta_1(\tau+i\gamma)\vartheta_2(\tau-i\alpha)\vartheta_2(\tau+i\beta)+\left(1-\sqrt{\varepsilon}\right)\exp(-\pi\tau i)\vartheta_1(\tau-i\gamma)\vartheta_2(\tau+i\alpha)\vartheta_2(\tau-i\beta)}{\vartheta_0(\tau)\vartheta_1(\tau)\vartheta_3(\tau)\Delta(\tau)},$$
$$\frac{dz}{d\tau} = iM \tag{3}$$
$$\times \frac{\left(1+\sqrt{\varepsilon}\right)\exp(\pi\tau i)\vartheta_1(\tau+i\gamma)\vartheta_2(\tau-i\alpha)\vartheta_2(\tau+i\beta)-\left(1-\sqrt{\varepsilon}\right)\exp(-\pi\tau i)\vartheta_1(\tau-i\gamma)\vartheta_2(\tau+i\alpha)\vartheta_2(\tau-i\beta)}{\vartheta_0(\tau)\vartheta_1(\tau)\vartheta_3(\tau)\Delta(\tau)},$$
$$\Delta(\tau) = \sqrt{1-\left(1-k'^2A^2\right)\mathrm{sn}^2(2K\tau,k)}.$$

Here, $M > 0$, ϑ_0 and ϑ_3 are zero and third theta-functions [12], $\mathrm{sn}(u,k)$ is an elliptical Jacobi sine, and $A = \mathrm{sn}(2Ka,k')$.

To determine the constant of simulation M, let us use the following ideas [16]. When point τ travels around point B along quadrant C_r with sufficiently small radius r (i.e., when vector $0.5(1+\rho i) - r = re^{i\Theta}$ turns and changes its argument Θ from -0.5π to $-\pi$), the respective point z should pass from ray AB to ray BC and the z increment should differ insignificantly from $-iT$:

$$\Delta z = -iT + O(r), \tag{4}$$

where $O(r)$ is infinitesimal as $r \to 0$.

On the other hand, under such a small increment $\Delta\tau$, the increment of function z is also small (in our case $dz/d\tau$ (3) is continuous at point $\tau = 0.5(1+\rho i)$). Therefore,

$$\Delta z = \int_{C_r}\frac{dz}{d\tau}dt = -iM\frac{\pi(1-\varepsilon)^{1/2}k\exp\pi(0.5\rho+\alpha-\beta-\gamma)\vartheta_3(i\gamma)\vartheta_0(i\alpha)\vartheta_0(i\beta)}{k'\sqrt{1-A^2}\vartheta_2(0)\vartheta_3(0)\vartheta_1'(0)} + O(r). \tag{5}$$

If we equate (4) and (5), obtained for Δz, and pass to the limit under $r \to 0$, we determine

$$M = \frac{\left(1-A^2\right)^{1/2}\exp\pi(\beta+\gamma-\alpha-0.5\rho)\vartheta_0^3(0)\vartheta_0^2(0)}{(1-\varepsilon)^{1/2}\vartheta_3(i\gamma)\vartheta_0(i\alpha)\vartheta_0(i\beta)}T. \tag{6}$$

Here, we use the known result [12]

$$\vartheta_1'(0) = \pi\vartheta_0(0)\vartheta_2(0)\vartheta_3(0).$$

If we write Eq. (3) for different boundary segments of area τ and perform integration along the entire boundary of the auxiliary area (Fig. 3), we close the area of motion z. As a result, we generate the expression for the main geometrical and filtration performances

$$\int_g^a Y_{GA}dt = S,\ -\int_0^{0.5}\Phi_{AB}dt = H,\ T - H_0 - d + \int_0^a \Phi_{FA}dt = H_0,$$
$$\lim_{\sigma\to 0}\left(\int_0^{0.5-\sigma}X_{DF}dt - \int_0^{0.5\rho-\sigma}X_{CD}dt\right) = L_1,\ \int_a^{0.5\rho}\Psi_{AB}dt = Q,\ d = T - H_0 - \int_0^{0.5}\Phi_{DF}dt, \tag{7}$$

for points coordinates of the free surface DF

$$x_{DF}(t) = \int_t^{0.5}X_{DF}dt,\ y_{DF}(t) = -d + \int_t^{0.5}Y_{DF}dt. \tag{8}$$

In formulas (7) and (8) the subintegral functions are the expressions in the right-hand side of Eq. (3) at the respective boundary segment of plane τ.

4. LIMIT CASE. CASES WITHOUT UPTHRUST AND INCLUSIONS

First of all, let us examine the case when $H_0 = 0$, i.e., there is no upthrust caused by the underseam underground water. Analysis shows that if we fix all the physical parameters of the scheme and if the head of the curve in the a permeable underseam decreases, the inflection point of depression curve E moves along the boundary towards point D and coincides with it at the limit under $\gamma = \gamma_* = 0$. Under such γ, the

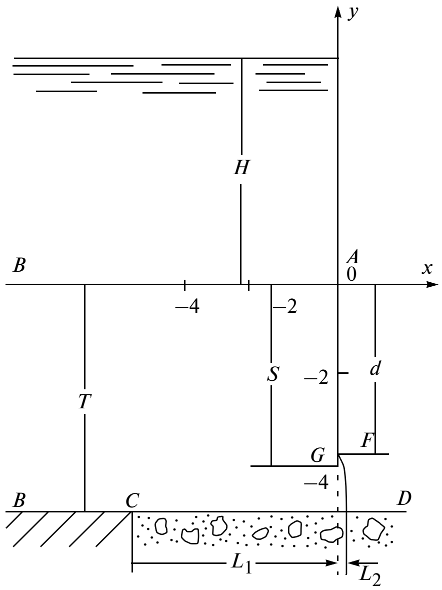

Fig. 4. The flow pattern calculated under the following parameters $\varepsilon = 0.5$, $H = 5$, $T = 5$, $S = 4$, $Q = 6.5$ and $L_1 = 4.5$.

right part of semicircle $|w - 0.5(1+\varepsilon)i| < 0.5(1-\varepsilon)$ (dashed line in Fig. 2) drops out of the area of complex velocity w, which is bifoliate, and in the flow plane z, the free surface flattens at point D and comes out to the roof of the water-permeable layer at a right angle to the abscissa equal to L_2, where L_2 is the projection of the curve of the depression to the x axis (Fig. 4). The solution for this limit case is determined from Eqs. (2)–(8), if we accept that $\gamma = 0$.

If in the plane of motion z points B and C coincide at infinity, it corresponds to the case when the impermeable inclusion, which is on the underseam of the roof of very permeable ground, disappears ($L_1 = \infty$). In this case, the rectangle for the plane of auxiliary variable τ transforms into semiband $0 < \operatorname{Re}\tau < 0.5$, $0 < \operatorname{Im}\tau < \infty$, since $k = 0$, $k' = 1$, $K = \pi/2$, and $K' = \infty$, and therefore $\rho = \infty$.

From the analysis it follows that if we fix all physical parameters of the scheme, and if the width of the impermeable inclusion decreases, point C moves along the boundary of area z towards point B and coincides with it at infinity at $\beta = \beta_* = 0.5\rho$. For such β, the second sheet of the Riemann surface in the area of complex velocity w degenerates into point B, which jointly with point A, passes to a certain point (for which $v_y = H/T > 1$) to the bottom sheet (Fig. 2).

The solution for this limit case is obtained from Eqs. (2)–(8), if we accept that $k = q = 0$ and consider that under $\beta = \beta_*$ [15]

$$\vartheta_2\left(\tau \pm i\beta_*\right) = \vartheta_2\left(\tau \pm i\rho/2\right) = q^{-1/4}\exp\left(\mp\pi\tau i\right)\vartheta_3(\tau).$$

In this case, the series for theta-functions is cut at the first members, elliptical functions degenerate into trigonometric ones, and expressions (2) and (3) can be written as follows:

$$w = i\sqrt{\varepsilon}\,\frac{\sin 2\pi\tau + 2i\sqrt{\varepsilon}\left[\operatorname{ch}\pi\gamma\operatorname{sh}\pi\alpha\operatorname{ch}^{-1}\pi(\alpha-\gamma) - \sqrt{\varepsilon}\cos^2\pi\tau\right]}{\sqrt{\varepsilon}\sin 2\pi\tau + 2i\left[\operatorname{ch}\pi\gamma\operatorname{sh}\pi\alpha\operatorname{ch}^{-1}\pi(\alpha-\gamma) - \sqrt{\varepsilon}\cos^2\pi\tau\right]},$$

$$\frac{dz}{d\tau} = \frac{\sqrt{\varepsilon}\sin 2\pi\tau + 2i\left[\operatorname{ch}\pi\gamma\operatorname{sh}\pi\alpha\operatorname{ch}^{-1}\pi(\alpha-\gamma) - \sqrt{\varepsilon}\cos^2\pi\tau\right]}{\Delta(\tau)},$$

$$\frac{dw}{d\tau} = -\sqrt{\varepsilon}M\,\frac{\sin 2\pi\tau + 2i\sqrt{\varepsilon}\left[\operatorname{ch}\pi\gamma\operatorname{sh}\pi\alpha\operatorname{ch}^{-1}\pi(\alpha-\gamma) - \sqrt{\varepsilon}\cos^2\pi\tau\right]}{\Delta(\tau)},$$

$$\Delta(\tau) = \sin\pi\tau\sqrt{\operatorname{ch}^2\pi a - \sin^2\pi\tau}.$$

The correspondence of points G in planes w and τ results in the following relationship

$$\operatorname{sh}\pi g = \frac{\operatorname{ch}\pi\gamma\operatorname{sh}\pi\alpha}{\operatorname{sh}\pi(\alpha-\gamma)}\exp(\pi g),$$

which makes it possible to determine parameter g. Under $\gamma = 0$, equation $\operatorname{sh}\pi g = \exp(\pi g)$ can be solved graphically.

5. NUMERICAL CALCULATIONS AND COMPARISON WITH THE RESULTS OBTAINED IN [1]

Formulas (2)–(8) contain 5 unknown constants: ordinates a and g for points A and G images in plane τ, parameters of conformal mapping α and β, and also module k. The first five equations in (7) and the following expressions are used to determine the unknown values and also to check the calculations

$$(1/w)|_G = 0, \qquad \int_0^{0.5}(\Phi_{DF} - \Phi_{BC})dt + \int_0^{a}\Phi_{FA}dt = 0$$

Table 1. The results of the calculation for d and L_2, if ε, L_1 and Q are varied

ε	d	L_2	L_1	d	L_2	Q	d	L_2
0.1	3.8459	0.0521	4.35	3.9227	0.1169	6.47	3.7091	0.0292
0.3	3.8059	0.0476	4.40	3.8639	0.0869	6.50	3.7584	0.0432
0.5	3.7584	0.0432	4.45	3.8070	0.0637	6.56	3.8441	0.0669
0.7	3.7092	0.0386	4.50	3.7584	0.0432	6.62	3.9060	0.0869
0.9	3.6602	0.0341	4.58	3.6814	0.0194	6.67	3.9485	0.0997

Table 2. The results of the calculation for d and L_2, if H, S, and T are varied

H	d	L_2	S	d	L_2	T	d
4.9	3.7888	0.0291	3.4	3.1621	0.0509	4.2	2.9584
5.0	3.7584	0.0432	3.8	3.5356	0.0469	4.6	3.3584
5.5	3.6312	0.1984	4.2	3.9763	0.0385	4.8	3.35584
6.0	3.5566	0.3959	4.6	4.4090	0.0255	5.0	3.7584
6.5	3.5136	0.6189	4.8	4.6572	0.0158	5.2	3.9584

(the first equation means that the velocity at the rabbet's end is equal to infinity, and the second one follows directly from the boundary conditions). When the unknown constants have been determined, we find value d (the last equation in (7)) and calculate the coordinates of the points for the depression curve according to formulas (8)–(12).

Let us estimate how physical parameters of the model ε, L_1, Q, H, T, and S influence sizes d and L_2. For this purpose, we examine the case when there is no upthrust caused by the underseam, i.e., when $H_0 = 0$. Figure 4 depicts the flow pattern, calculated under the following parameters: $\varepsilon = 0.5$, $L_1 = 4.5$, $Q = 6.5$, $H = 5$, $S = 4$, and $T = 5$ (basic values). Tables 1 and 2 present the results of the calculation that show how physical parameters of the scheme influence sizes d and L_2. Figure 5 depicts the relationship between d (curve *1*) and L_2 (curve *2*), as well as parameters ε, H, and S.

Analyzing the information presented in Tables 1 and 2 and in the plots, it is possible to make the following conclusions.

If seepage and upthrust intensities are increased and the width of the impermeable inclusion, seepage flow rate, the rabbet's length, and layer power are decreased, the value of d drops; i.e., the ordinate of point F, where the depression curve comes out of the rabbet, increases. According to the information presented in Table 1, if parameters L_1 and Q are changed by a factor of 1.1, value d decreases 6.5%. The layer power T significantly influences size d. From Table 2 it is seen that if T is increased by a factor of 1.2, value d increases by 33.8%. It is seen that d varies linearly with T.

As for the value L_2, it increases, if the upthrust, seepage flow rate and the width of impermeable inclusion are increased, and it decreases, if the seepage intensity and the rabbet's length are increased. In this case, parameter L_2 is the most dependent on width L_1 and upthrust H: if values L_1 and H are varied by a factor of 1.1 and 1.3, respectively, the projection of the free surface changes by 502.4 and 2025.3%, respectively. As shown in [1], the layer's power influences insignificantly on L_2: if parameter T is varied for the variants, which are presented in the right part of Table 2, we have the same value of $L_2 = 0.0432$.

We see different behavior for parameters d and L_2, if H and S are varied (Table 2) and, vice versa, a similar qualitative character for the relationships between these sizes and ε and L_1 (Table1): if the last parameters are decreased, the ordinate of the point at which the ground water comes out of the rabbet decreases and the projection of the depression curve increases. If we compare the obtained results with the results for the case when the velocity of the flow at the end of the rabbet meets the condition $|\bar{v}_G| < \varepsilon$ [1], we see that the relationships between d and L_2 and parameters H, S, and T (Fig. 5) are similar qualitatively.

The most interesting is the case when we vary width L_1 for the segment of a very permeable layer adjacent directly to the impermeable inclusion BC, which characterizes the position of point C. The results of the calculations (Table 1) show that if parameter L_1 is increased; i.e., if point C moves away from ordinate

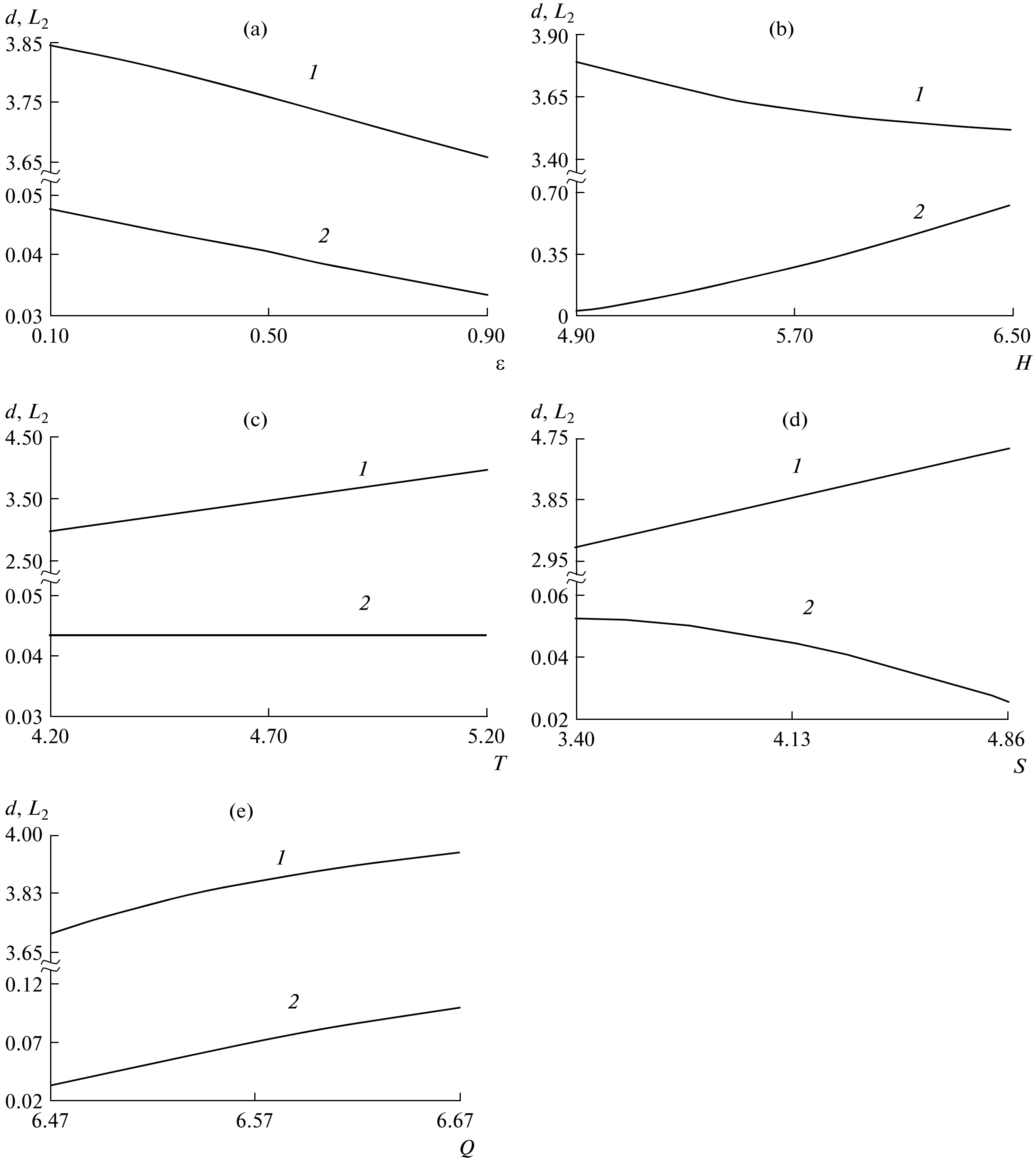

Fig. 5. Relationships between d (*1*), L_2 (*2*) and (a) under constant $H = 5$, $T = 5$, $S = 4$, $Q = 6.5$, and $L_1 = 4.5$; and H (b) under constant $\varepsilon = 0.5$, $T = 5$, $S = 4$, $Q = 6.5$, and $L_1 = 4.5$; and T (c) under constant $\varepsilon = 0.5$, $H = 5$, $S = 4$, $Q = 6.5$, $L_1 = 4.5$; and S (d) under constant $\varepsilon = 0.5$, $H = 5$, $T = 5$, $Q = 6.5$, and $L_1 = 4.5$; and Q (e) under constant $\varepsilon = 0.5$, $H = 5$, $T = 5$, $S = 4$, and $L_1 = 4.5$.

axis (to the left), the projection of the free surface L and value d decrease. The calculations also show that in contrast to the case when the flow velocity is finite, for which point C (the right end of the impermeable inclusion) is always to the right of the ordinate axis [1], in the examined model it is to the left.

REFERENCES

1. E. N. Bereslavskii, L. A. Aleksandrova, E. V. and Pesterev, “On Ground Water Seepage under Hydraulic Structures,” Math. Models Comput. Simulations **3** (5), 619 (2011).
2. P. Ya. Polubarinova-Kochina, *The Theory of Ground Water Motion* (Nauka, Moscow, 1977) [in Russian].
3. P. Ya. Kochina, *Selected Works. Hydrodynamics and Seepage* (Nauka, Moscow, 1991) [in Russian].
4. E. N. Bereslavskii, “On Fuchs Differential Equations Connected with Conformal Mapping for Round Polygons in Polar Grids,” Differents. Uravn. **33** (3), 296–301 (1997).
5. E. N. Bereslavskii, “How to Integrate in Closed Form Some Fuchs Differential Equations that Take Place in Hydro and Aeromechanics,” Dokl. Akad. Nauk **428** (4), 439–443 (2009).
6. E. N. Bereslavskii, “How to Integrate in Closed Form Some Fuchs Differential Equations Connected with Conformal Mapping of Round Pentagons with Cuts,” Differents. Uravn. **46** (4), 459–466 (2010).
7. E. N. Bereslavskii and P. Ya. Kochina, “Several Fuchs Equations in Hydro and Aeromechanics,” Izv. Akad. Nauk. Mekh. Zhidk. Gaza, No. 5, 3–7 (1992).
8. P. Ya. Kochina, E. N. Bereslavskii, and N. N. Kochina, “Analytical Theory of Fuchs Linear Differential Equations and Some Problems of Underground Hydromechanics. Part 1,” Preprint No. 567 (Institute for Problems in Mechanics of the Russian Academy of Sciences, Moscow, 1996).
9. E. N. Bereslavskii and P. Ya. Kochina, “On Fuchs Differential Equations in Several Problems of Fluid Mechanics,” Izv. Akad. Nauk. Mekh. Zhidk. Gaza, No. 5, 9–17 (1997).
10. V. Koppenfels and F. Stahlmann, *Practice of Conformal Mapping* (Inostr. lit., Moscow, 1963).
11. E. N. Bereslavskii, “On Conformal Mapping of Several Round Polygons to Rectangle,” Izv. Vyssh. Uchebn. Zaved. Mat., No. 5, 3–7 (1980).
12. I. S. Gradshtein and I. M. Ryzhik, *Tables for Integrals, Sums, Series and Products* (Nauka, Moscow, 1971) [in Russian].
13. *Seepage Theory Development in the USSR (1917–1967),* Ed. by P. Ya. Polubarinova-Kochina (Nauka, Moscow, 1969) [in Russian].
14. G. K. Mikhailov and V. N. Nikolaevskii, “Fluids Motion in Porous Mediums,” in *Mechanics in the USSR for 50 Years* (Nauka, Moscow, 1970), Vol. 2, pp. 585–648.
15. V. V. Golubev, *Lectures on Analytical Theory for Differential Equations* (Gostekhizdat, Moscow–Leningrad, 1950) [in Russian].
16. M. A. Lavrent’ev and B. V. Shabat, *Methods of Complex Variable Theory* (Nauka, Moscow, 1987) [in Russian].